In Vivo Multiphoton NADH Fluorescence Reveals Depth-Dependent Keratinocyte Metabolism in Human Skin

Mihaela Balu,[†] Amaan Mazhar,[‡] Carole K. Hayakawa,[†§] Richa Mittal,[†§] Tatiana B. Krasieva,[†] Karsten König,[¶||] Vasan Venugopalan,[†§**] and Bruce J. Tromberg[†***]

[†]Laser Microbeam and Medical Program (LAMMP), Beckman Laser Institute and Medical Clinic, University of California, Irvine, California; [‡]Modulated Imaging, Irvine, California; [§]Department of Chemical Engineering and Materials Sciences, Irvine, California; [¶]JenLab GmbH, Jena, Germany; [||]Department of Biophotonics and Laser Technology, Saarland University, Saarbrücken, Germany; and **Department of Biomedical Engineering, University of California, Irvine, California

ABSTRACT We employ a clinical multiphoton microscope to monitor in vivo and noninvasively the changes in reduced nicotinamide adenine dinucleotide (NADH) fluorescence of human epidermal cells during arterial occlusion. We correlate these results with measurements of tissue oxy- and deoxyhemoglobin concentration during oxygen deprivation using spatial frequency domain imaging. During arterial occlusion, a decrease in oxyhemoglobin corresponds to an increase in NADH fluorescence in the basal epidermal cells, implying a reduction in basal cell oxidative phosphorylation. The ischemia-induced oxygen deprivation is associated with a strong increase in NADH fluorescence of keratinocytes in layers close to the stratum basale, whereas keratinocytes from epidermal layers closer to the skin surface are not affected. Spatial frequency domain imaging optical property measurements, combined with a multilayer Monte Carlo-based radiative transport model of multiphoton microscopy signal collection in skin, establish that localized tissue optical property changes during occlusion do not impact the observed NADH signal increase. This outcome supports the hypothesis that the vascular contribution to the basal layer oxygen supply is significant and these cells engage in oxidative metabolism. Keratinocytes in the more superficial stratum granulosum are either supplied by atmospheric oxygen or are functionally anaerobic. Based on combined hemodynamic and two-photon excited fluorescence data, the oxygen consumption rate in the stratum basale is estimated to be ~0.035 μmoles/10^6 cells/h.

INTRODUCTION

Real-time, in vivo noninvasive monitoring of the supply of oxygen to the mitochondria within epidermal cells is important for clinical purposes and for understanding of cellular physiology and cytology. One way to evaluate the supply of oxygen within cells is by monitoring the amount of reduced nicotinamide adenine dinucleotide (NADH) within mitochondria. NADH, one of the major mitochondrial components, plays a key role in cellular energy metabolism. During the metabolic process, it drives the electron transport chain (ETC), the final stage of cellular respiration, in the presence of oxygen. NADH is intrinsically fluorescent and a well-established indicator of mitochondrial oxygen supply (1,2).

Monitoring and imaging mitochondrial NADH fluorescence is an area that has grown substantially over the last 50 years. A recent review (3) summarizing these studies shows that changes in NADH fluorescence due to oxygen deprivation have been measured in single cells (4), in tissue slices (5), and organs in vitro (6,7) and in vivo (8,9). Nevertheless, only a few studies have reported findings related to changes in NADH fluorescence due to reduction of oxygen supply in skin, the largest organ of the human body. One of the earliest attempts to monitor the oxygen supply within the epidermis was performed by Chance and co-workers (10) who showed, by using ultraviolet (UV) excitation-based fluorescence spectrophotometry, that rat skin slices undergo changes in NADH fluorescence during anoxia. Cordeiro et al. (11) have shown that fluorescence spectroscopy of endogenous NADH is a sensitive and reliable indicator of vascular occlusion in porcine myocutaneous flaps. These pioneering studies based on UV excitation sources provide the groundwork for further exploration of cellular metabolism using near-infrared (NIR) excitation-based nonlinear microscopy and spectroscopy.

Two-photon excited fluorescence (TPEF) employing NIR excitation sources has the advantage of reduced cellular photodamage and improved cell viability compared to UV-based one-photon excitation, allowing in vivo probing of mitochondrial NADH fluorescence over an extended period of time. Additionally, due to lower scattering of the near infrared light compared to UV light, TPEF microscopy permits deeper penetration into thick, highly scattering tissues. This method has been instrumental in evaluating in vivo the behavior of protein-bound and free NADH in rat skin during ischemia (12). Another recent study of NADH fluorescence in epidermal cells during oxygen deprivation showed the metabolic deterioration of ex vivo human skin from ischemic necrosis (13). Although TPEF capabilities for monitoring cellular metabolism in animal skin (in vivo) and human skin (ex vivo) are promising, moving this technology to in vivo imaging of human skin would allow noninvasive, real time assessment of epidermal cell metabolism. In addition to its potential applicability in

Submitted June 22, 2012, and accepted for publication November 26, 2012.

*Correspondence: bjtrombe@uci.edu

Editor: David Piston.

0006-3495/13/01/0258/10 $2.00

http://dx.doi.org/10.1016/j.bpj.2012.11.3809

clinical practice, this technique used in vivo on human skin could address controversies such as the significance of atmospheric oxygen contribution to the oxygen supply of human epidermis (14) or the proposed anaerobic metabolism of human epidermis (15).

Translation of TPEF to clinical practice has been limited due to challenges related to the large footprint of laser scanning microscopes and ultrafast laser sources, the lack of a stable, flexible patient interface for scanning any region of the body, and blurring effects due to physiological motion artifacts. Many of these challenges have been resolved with the recent development of a portable, clinical multiphoton tomograph (MPTflex, JenLab GmbH, Jena, Germany) the successor model of JenLab's DermaInspect system (16).

In this work, we employ the MPTflex to monitor in vivo and noninvasively the changes in NADH fluorescence of human epidermal cells under conditions of blood-supplied oxygen deprivation. Ischemia-induced changes in NADH fluorescence of keratinocytes in layers close to the stratum basale are compared to NADH fluorescence of keratinocytes from epidermal layers closer to the skin surface. We correlate these results with quantitative dynamic measurements of tissue oxy- and deoxyhemoglobin concentration during oxygen deprivation (cuff occlusion) using spatial frequency domain imaging (SFDI) (17).

To confirm that the observed change in NADH fluorescence is a true indicator of the cellular metabolic state rather than an artifact of possible tissue optical property changes during ischemia, we analyzed the tissue absorption and scattering coefficients obtained during SFDI measurements throughout the occlusion. These data were used to determine whether there were significant changes in optical properties in the 450–550 nm NADH emission range. We also established a 7-layer Monte Carlo-based radiative transport model of multiphoton microscopy (MPM) signal collection in skin. The model accounts for localized changes in tissue absorption and scattering and their impact on NADH fluorescence collection. Both model and experimental results confirm that the impact of optical property changes on NADH fluorescence during cuff occlusion is negligible. As a result, we are able to directly correlate measurements of keratinocyte NADH fluorescence with tissue hemodynamics and estimate the intrinsic rate of cellular oxygen consumption close to the basal layer.

MATERIALS AND METHODS

MPTflex clinical tomograph

The laser scanning based clinical multiphoton tomograph as shown in Fig. 1, consists of a compact, turnkey femtosecond laser (MaiTai Ti:Sappire oscillator, sub-100 fs, 80 MHz, tunable 690–1020 nm; Spectra Physics, Mountain View, CA), an articulated arm with NIR optics and beam scanning module. The system has two photomultiplier tube detectors employed for parallel acquisition of second harmonic generation and TPEF signals. A customized metallic ring taped on the subject's skin attaches magnetically

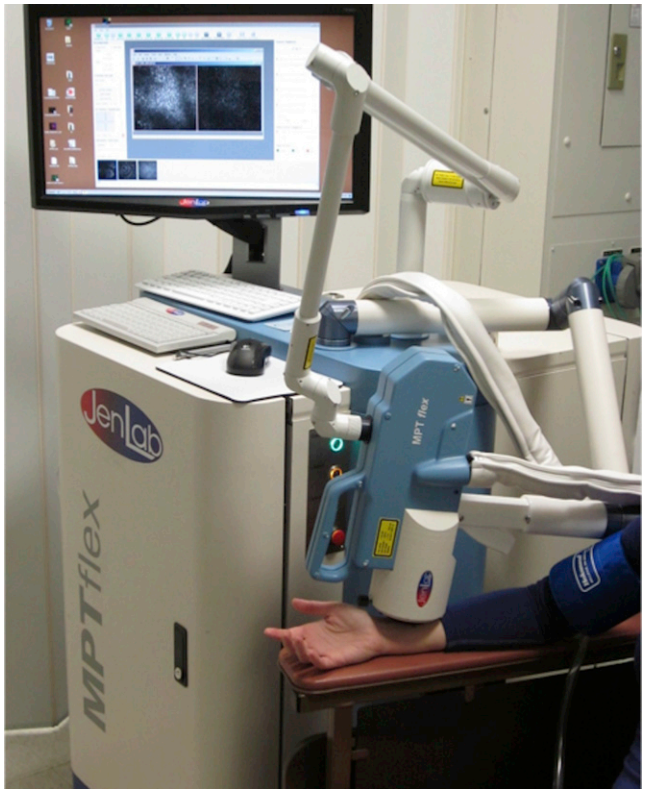

FIGURE 1 MPM-based clinical tomograph (MPTflex) during the occlusion experiment.

to the objective holder in the articulated arm, minimizing motion artifacts. In this work, the excitation wavelength was tuned to 765 nm for efficient excitation of NADH. The NADH fluorescence is detected over a broad spectral range (410–650nm) through emission filters placed in the TPEF detection channel.

Flavin adenine dinucleotide (FAD) can also contribute to the detected fluorescence signal in this excitation/emission spectral range. However, although FAD has a larger two-photon absorption cross section than NADH at 765 nm (18), it also has an extremely low fluorescence quantum yield, which is attributed to several factors including dynamic quenching by the adenine part of the molecule (19,20). This is the reason FAD does not generally contribute to fluorescence generated by two-photon excitation at wavelengths shorter than 780 nm, as previously reported (18,21,22). Nevertheless, the presence of a small FAD fluorescence background might be possible in our detected wavelength range. As we will show and discuss below, an increase in the NADH fluorescence signal was measured during the occlusion. If there is indeed an FAD fluorescence contribution, the increase in the NADH signal would be slightly underestimated as the two signals, NADH and FAD fluorescence respond in opposite directions to changes in mitochondrial metabolic states (18). Consequently, the absolute value of the NADH increase measured during occlusion might be slightly higher than the value we measured, but this does not affect the conclusions of our study. Keratin autofluorescence also contributes to the fluorescence signal detected on this channel. This has not been a concern for our measurements because our interest was to measure changes in NADH fluorescence due to blood-supplied oxygen deprivation rather than absolute values. In this work, the second harmonic generation channel was used only for proper identification of the epidermal-dermal junction. We used a Zeiss objective (40X, 1.3NA, oil immersion) for focusing into the tissue. The laser power at the surface of the skin was 5 mW and the pixel dwell time 26 μs.

SFDI instrument

The SFDI instrument consists of three fundamental components: a light source, spatial light modulator, and camera. For these studies, a prototype clinic-compatible system (Modulated Imaging, Irvine, CA) was used to measure tissue oxyhemoglobin (ctO_2Hb), deoxyhemoglobin (ctHHb), tissue oxygen saturation (stO_2) and the tissue optical properties—specifically, the quantitative absorption (μ_a) and reduced scattering (μ_s') parameters (23). Based on previous work (17) a light source consisting of modules with LED's centered at 658, 730, and 850 nm were implemented to optimize quantification of hemoglobin chromophores. A digital light projector based on a Digital Micromirror Device (Texas Instruments DMD Discovery 1100, Texas Instruments, Dallas, TX) is used to project patterns onto the sample. The detection arm consists of two cameras: a dedicated NIR camera and a color camera. White light is projected after each pass of data to capture a color photograph of the region of interest so that SFDI images can be compared at the exact same site on human skin. The projector and NIR detection arms are fitted with cross-polarizers to eliminate specularly reflected light. All system hardware is controlled by custom C# software (Modulated Imaging) connected to a PC computer via universal serial bus. In addition to SFDI data, a surface profilometry measurement is built into the acquisition to correct for optical property errors resulting from surface curvature, as described by Gioux et al. (24). Optical property determination, chromophore concentration map rendering, and image processing are done using MATLAB (The MathWorks, Natick, MA), which occurs offline, after data has been acquired. Representative SFDI images, corresponding to absorption and scattering maps and to quantitative oxy- and deoxyhemoglobin concentration maps, are shown in Fig. 2.

In vivo measurements and analysis

SFDI and TPEF images of a human volar forearm under blood-supplied oxygen deprivation conditions were acquired according to an approved UC Irvine institutional review board protocol. Both techniques were used successively to image a subject volar forearm for 9 min. Images were recorded before, during, and after occlusion for 3 min each. During occlusion an arm cuff was inflated to 220-mm Hg pressure on the subject's bicep to create an arterial-venous occlusion.

For monitoring the changes in cellular NADH fluorescence due to blood-supply oxygen deprivation, a time series of TPEF images corresponding to a fixed layer of epidermal cells was recorded during a 9 min occlusion experiment. The acquisition time was 6.2 s for each frame and 3.8 s between frames, corresponding to a 10 s time between consecutive frames and a total of 54 frames acquired in 9 min, the duration of one experiment. 512 × 512 images were recorded from two different epidermal layers, a deep epidermal layer (closer to the basal layer; 35–40 μm deep) and a more superficial skin layer (closer to skin surface; 20–25 μm deep) to compare how the two layers are affected by the occlusion. A control experiment was performed by recording a TPEF time series from the same layer of epidermal cells on the subject forearm under normal blood flow and oxygenation conditions. The acquisition time per frame was the same as for the occlusion experiment, but the total acquisition time was 6 min. Each experiment (control and occlusion) was repeated five times on the same subject. In each experiment, each frame was analyzed by calculating the mean intensity of the cellular fluorescence in a region of interest (ROI) that was the same for each frame and included the same cells in all the frames in the time series. Each ROI included ~15–20 cells. In each time series there were a few frames that corresponded to a slightly different layer than most of the other frames, due to motion artifacts, especially during the cuff inflation/deflation. These frames were not included in the analysis.

SFDI data were acquired at three wavelengths (658, 730, and 850) using four spatial frequencies spaced evenly between 0 and 0.15 mm^{-1}, interrogating a depth of 2–3 mm. Data were acquired every 10 s before occlusion (baseline), during occlusion, and release. Only two frequencies (0 and 0.15 mm^{-1}) were used to process the data so that the impact of motion artifacts could be minimized. SFDI data were processed using a height correction algorithm described previously (24). A one layer Monte Carlo model of light propagation in the spatial frequency domain was used, allowing analysis of reflectance for a wide span of optical properties. We have shown in previous work that absorption and scattering maps can be rapidly determined by measuring reflectance at two spatial frequencies using a precomputed lookup table, a computational optimization of a two-frequency nonlinear least squares model-based analysis (25). The absorption maps were then used to fit for chromophores concentrations oxyhemoglobin (ctO_2Hb) and deoxyhemoglobin (ctHHb) using LED corrected basis spectra. The fields of view corresponding to SFDI and TPEF measurements were 14 × 10 cm^2 and 150 × 150 μm^2, respectively. A smaller region of interest (ROI = 5 × 2 cm^2) corresponding to an area with microvasculature prominence on the forearm was selected for SFDI analysis. The ROI corresponding to the SFDI measurement was selected to include the microscopic

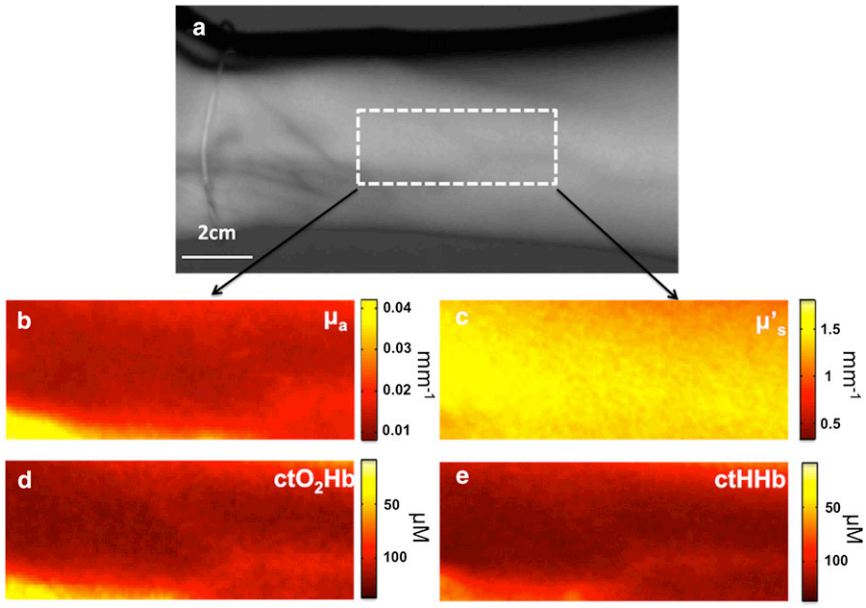

FIGURE 2 (*a*) Reflectance map at 850 nm including the ROI selected for the SFDI analysis. SFDI absorption (*b*) and scattering (*c*) maps corresponding to 850 nm. SFDI quantitative oxyhemoglobin (*d*) and deoxyhemoglobin (e) concentration maps.

area imaged with TPEF. The microvasculature area selected for both SFDI and TPEF provided more stable measurements than the areas close to veins.

The oxygen consumption (OC) rate by basal layer keratinocytes was estimated from the correlation of changes in NADH fluorescence with changes in vascular hemoglobin during arterial occlusion. The rate of decrease in oxyhemoglobin concentration (ctO_2Hb) is related to the rate of OC concentration by

$$OC = -4\frac{\partial}{\partial t}ctO_2Hb, \quad (1)$$

where the 4 accounts for the hemoglobin/oxygen molar ratio (26). The OC calculated by using the previous equation is expressed in μmoles per unit volume per unit of time. To estimate the OC per cell per unit of time, we calculated the average number of cells in the imaged volume.

Monte Carlo model

A 7-layer skin model with an embedded isotropic point source was developed to simulate the impact of intrinsic optical property changes on the NADH fluorescence emission (Fig. 3). The model is similar to that introduced by Meglinski (2002) (27) and provides layer thicknesses, refractive index, and anisotropy coefficient for each layer. The absorption coefficient for each layer is calculated using the volume fractions of blood, water, blood oxygen saturation, and melanin. The scattering coefficients given in the Meglinski model were those at $\lambda = 632.8$ nm and we used scattering data provided in Van Gemert (1989) (28) to extrapolate the scattering coefficient to the wavelengths of interest. The source was placed at a location in the epidermis 35 μm below the tissue surface, which was the approximate depth that we imaged the NADH fluorescence in keratinocytes during occlusion. We used a 1 mm diameter detector corresponding to the size of the collection area of the objective used for the MPM imaging. The Monte Carlo simulations were performed using the Virtual Tissue Simulator (29). The photons were launched isotropically from the fluorescent source, and propagated within a conventional Monte Carlo simulation (30) using discrete absorption weighting, which decrements the photon weight at each collision by the ratio of the scattering coefficient to the total attenuation coefficient (μ_s/μ_t).

We generated Monte Carlo interrogation maps, subdividing the tissue into three-dimensional voxels, to understand how the light interrogates various regions in the tissue before detection (31). For those photons that exit the tissue and enter the detector, we rewound the photon's trajectory back to the source, determined which voxels the photon visited before detection, and added the photon's detected weight into the voxel. This provided the probability of visitation and detection given by Bayes's theorem, $P(V\&D) = P(V)\,P(D|V)$. The photon weight upon visiting each voxel gives $P(V)$ and the contribution to $P(D|V)$ is the weight change from visitation to detection. The product of these two factors is equal to the final weight of the photon upon detection. The voxel sums after N launched photons is then normalized by dividing by N. We used $N = 10^6$ photons launched from the source for all simulations.

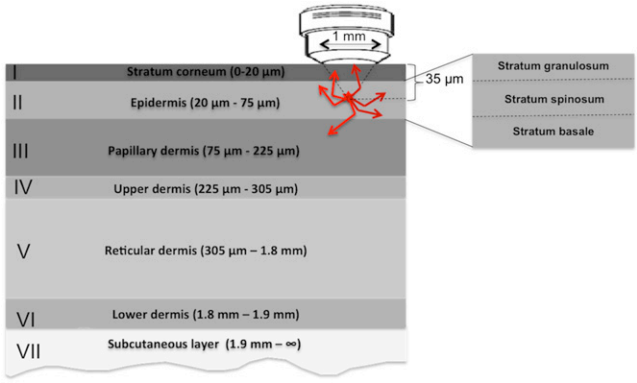

FIGURE 3 Schematic 7-layer Monte Carlo model of skin with dermis subdivided into four layers with different blood volume fractions. The NADH fluorescence source was placed at a location in the epidermis 35 μm below the tissue surface, and a 1 mm diameter detector was used corresponding to the size of the collection area of the objective (see text).

RESULTS AND DISCUSSION

Cellular respiration occurs in three stages: glycolysis, Krebs cycle, and ETC. The NADH molecules, produced in the glycolysis stage and in the Krebs cycle, are fed into the ETC where they are used in the process of oxidative phosphorylation (OXPHOS) to produce ATP, the main energy-storing molecule. In the OXPHOS process, the electrons flow from electron donors such as NADH to electron acceptors such as oxygen. Whereas the NADH is the first electron donor, the oxygen is the final electron acceptor in the chain. Deficiency of oxygen reduces the flow of electrons and slows down the OXPHOS process. As a consequence of the deceleration of the OXPHOS process, the rate of the NADH conversion to NAD^+ in the first reaction of the ETC decreases, resulting in a higher concentration of NADH. Therefore, the NADH concentration is closely related to the cellular oxygen supply (2,32).

The mechanism of oxygen exchange in human skin has been investigated theoretically and experimentally. Theoretical studies based on loop-shaped capillary models have predicted an even contribution of atmospheric and vascular oxygen to the epidermis (33,34). Experimental studies based on local measurements of the changes in cutaneous uptake of oxygen from atmosphere also suggest that the epidermal oxygen uptake from the atmosphere is in balance with the capillary oxygen supply (35). These studies estimate that the total thickness of the skin supplied by external oxygen is ~266–375 μm (14). Another hypothesis recently advanced is that keratinocytes, at least those above the basal layer, are not very likely to engage in the OXPHOS process being functionally anaerobic as the keratinocytic mitochondria are metabolically dysfunctional (15). Contrary to these hypotheses, a recent study of in vivo NADH fluorescence during ischemia in mouse keratinocytes, showed a metabolic response of keratinocytes in the stratum basale and stratum spinosum to complete deprivation of blood-supplied oxygen (12).

Here, we use a clinical multiphoton tomograph to monitor in vivo the metabolic response of human keratinocytes to induced ischemia through blood-supplied oxygen deprivation. First, a control experiment was performed by recording a time series of TPEF images corresponding to the same layer of epidermal cells on the subject forearm under normal blood flow and oxygenation conditions. Representative TPEF images of human epidermal cells at different time points (2, 4, and 6 min) in the time series of one of the

five experiments are presented in Fig. 4, *a*–*c*. The mean intensity was calculated for each image in the time series. The intensity results from five experiments were averaged and plotted as a function of time in Fig. 4 along with the corresponding standard deviation for each time point. The random fluctuation in the TPEF signal can be attributed to possible variations in NADH fluorescence in the same cell. Although care has been taken to only analyze images from the same epidermal layer in each time series, there are always small variations in images due to motion artifacts that can contribute to fluctuations of the TPEF signal.

The results of the in vivo occlusion experiment using TPEF microscopy and SFDI are presented in Fig. 5. In the TPEF microscopy experiment, the time series for each layer of epidermal cells were recorded before, during, and after arterial occlusion. The mean intensity was calculated for each image in the time series. The intensity results from five experiments were averaged and plotted as a function of time in Fig. 5 along with the corresponding standard deviation for each time point. The intensity results presented in Fig. 5 *a* correspond to images of keratinocytes in a layer close to the skin surface (stratum granulosum, ~20–25 μm deep). Representative TPEF images of keratinocytes from this layer at different time points (before, during, and after occlusion) for one of the five experiments are presented in Fig. 5, *a*1, *a*2, and *a*3. The intensity results presented in Fig. 5 *b* correspond to images of keratinocytes in a layer close to stratum basale (~35–40 μm deep). Representative TPEF images of keratinocytes from this layer at different time points (before, during, and after occlusion) for one of the five experiments are presented in Fig. 5, *b*1, *b*2, and *b*3.

The results show that ischemia induced by blood-supplied oxygen deprivation is associated with a strong increase in NADH fluorescence of keratinocytes in layers close to the stratum basale, whereas keratinocytes from epidermal layers closer to the skin surface are not affected. This implies that the metabolic processes of keratinocytes in deeper layers such as stratum spinosum and stratum basale are regulated by capillary oxygen supply, whereas the keratinocytes in upper layers such as stratum granulosum are either supplied by atmospheric oxygen (14) or are functionally anaerobic as suggested in previous studies (15). A statistical significance test over the $n = 5$ repeated measurements on one subject results in a p-value of 0.002, which indicates a significant increase of the NADH fluorescence signal during occlusion with respect to the value corresponding to normal blood flow.

Although other processes, such as the lack of glucose availability, can result from arterial occlusion, we believe oxygen deprivation is the main process that can lead to a significant increase in NADH. As shown in previous publications, NADH responds in the same direction as the change in glucose, i.e., an increase in glucose stimulates an increase in NADH fluorescence, whereas a decrease in glucose results in a reduction (21,36,37). In our experiment, the possible contribution of the lack of glucose to the change in NADH during occlusion would result in an underestimation of the NADH increase we measure during the occlusion. The absolute value of the NADH increase measured during occlusion might be higher than the value we measured, but this does not affect the conclusion of our study.

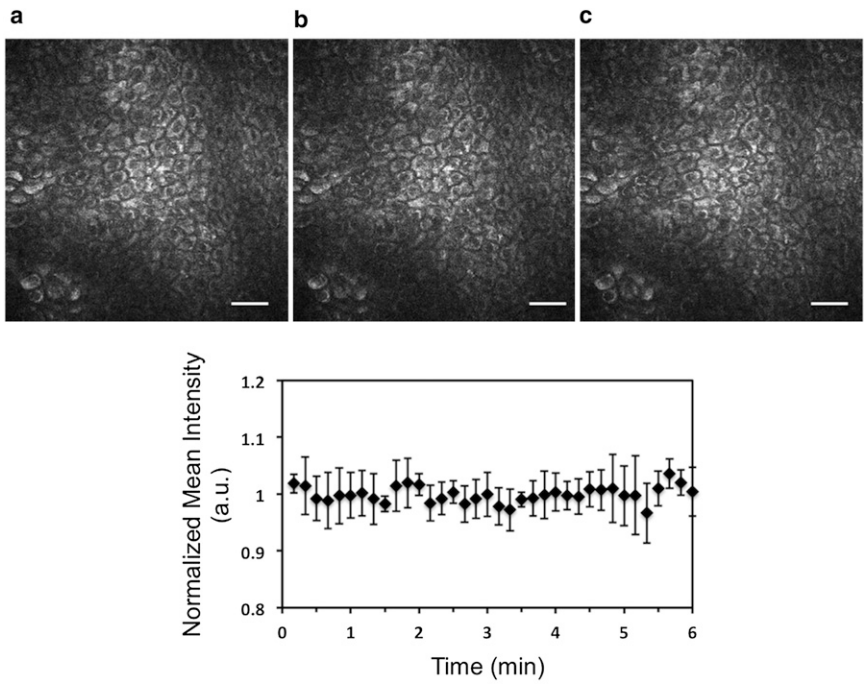

FIGURE 4 Representative TPEF in vivo images of human keratinocytes from time series corresponding to (*a*) $t = 2$ min (*b*) $t = 4$ min (*c*) $t = 6$ min. Scale bar is 20 μm. The graph represents the average of normalized mean intensities of TPEF images as a function of time. Error bars represent standard deviation.

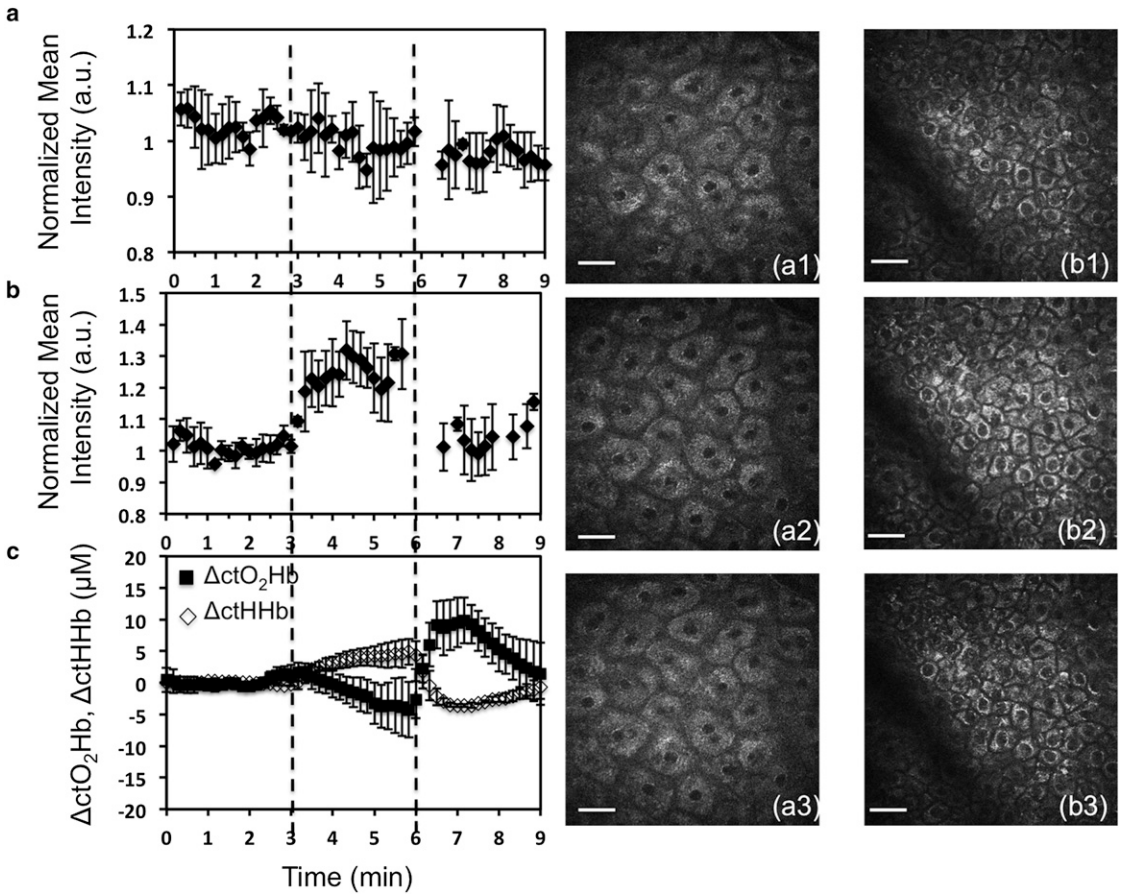

FIGURE 5 Normalized mean intensity of TPEF images as a function of time before, during, and after arterial occlusion for human keratinocytes in stratum granulosum (*a*) and in a layer close to stratum basale (*b*). Representative TPEF in vivo images recorded before (*a*1, *b*1), during (*a*2, *b*2), and after (*a*3, *b*3) occlusion corresponding to human keratinocytes in stratum granulosum (*a*1, *a*2, *a*3) and in a layer close to stratum basale (*b*1, *b*2, *b3*). Scale bar is 20 μm. (*c*) Hemodynamic response to arterial occlusion; oxyhemoglobin concentration ctO_2Hb (*square*), deoxyhemoglobin concentration ctHHb (*diamond*). The dashed lines represent the start and the release points of the occlusion. Error bars represent standard deviation.

Our in vivo results corresponding to an increase in NADH fluorescence in human keratinocytes close to the basal layer due to oxygen deprivation are similar to previous studies on isolated rat skin (10), in vivo mice skin (12), and ex vivo human skin (13). It has been shown that in mouse epidermal cells, ischemia results in the accumulation of NADH in Complex I leading to a strong increase in the protein-bound NADH fluorescence (12). Presently, we are not able to discriminate between fluorescence from free and protein-bound NADH. The addition of a fluorescence lifetime and/or spectral detection channel would make this possible.

The NADH fluorescence changes have been monitored concurrently with changes in tissue oxy- and deoxyhemoglobin concentration during oxygen deprivation using SFDI (Fig. 5 *c*). After the blood flow is occluded at $t = 3$ min, the tissue deoxyhemoglobin concentration (ctHHb) increases at the expense of oxyhemoglobin (ctO_2Hb), because oxygen is extracted from blood by the epidermal cells and surrounding tissue. The occlusion-induced ischemia reduces the rate of oxidative phosphorylation, resulting in a higher concentration of NADH and higher fluorescence from the epidermal cells that are sensitive to capillary oxygen supply. After the occlusion release at $t = 6$ min, the tissue is rapidly reperfused resulting in an increase in ctO_2Hb and decrease in ctHHb. There is an initial overshoot of the oxy and deoxyhemoglobin values followed by a return to baseline. These results are similar to previous in vivo measurements of human tissue hemodynamics during arterial occlusion using SFDI (17) and other techniques (38).

The rate of increase in NADH is ~4- to 5-fold faster than the rate of decrease in oxyhemoglobin. This is because the NADH fluorescence change is a consequence of a highly localized effect of oxygen depletion that occurs directly in the mitochondria. In contrast, the measured reduction in oxyhemoglobin is driven by an oxygen tension gradient that exists between the mitochondria and the microvascular supply. During arterial occlusion, persistent cellular oxygen demand produces ischemia. The slower rate of change of oxyhemoglobin therefore reflects the time required to

establish a diffusion gradient that is sufficient to drive the release of hemoglobin-bound oxygen from the vascular compartment.

The relationship between the hemodynamic changes and the changes in the NADH fluorescence intensity of the keratinocytes in the stratum spinosum during the arterial occlusion is shown in Fig. 6. The hemodynamic data represent the average results of the three SFDI experiments, whereas the NADH fluorescence intensity data correspond to one arbitrarily chosen MPM experiment. Fig. 6 *a* shows the dependence of the deoxyhemoglobin concentration on the NADH fluorescence intensity during the 3 min of arterial occlusion. Fig. 6 *b* shows the dependence of the hemoglobin oxygen saturation on the same parameter during the occlusion. These relationships imply that changes in NADH fluorescence can be a measure of the oxygen availability in the tissue, as previously suggested (9). It is expected these relationships would become sublinear at longer occlusion times due to consumption of all available oxygen supply, which leads to cessation of the oxidative phosphorylation process and no further changes in NADH. Fig. 6 *c* shows the dependence of the total hemoglobin concentration on the NADH fluorescence intensity. The change in total hemoglobin concentration is negligible because the decrease in oxyhemoglobin during the arterial occlusion is compensated by the increase in deoxyhemoglobin. Correlations between the changes of hemodynamic coefficients and the NADH fluorescence during occlusion were estimated by linear regression. The correlation coefficients for the deoxyhemoglobin R = 0.97 (Fig. 6 *a*), hemoglobin oxygen saturation R = 0.96 (Fig. 6 *b*), and total hemoglobin R = 0.12 (Fig. 6 *c*) correspond to *p*-values of 0.000012, 0.000015, and 0.4, respectively. The low R-value corresponding to the correlation coefficient for the total hemoglobin shows that the variation of the total hemoglobin is independent of the change in NADH fluorescence during occlusion. This is expected because the arterial-venous occlusion maintains a constant amount of hemoglobin in the arm by preventing blood flow perfusion and venous return.

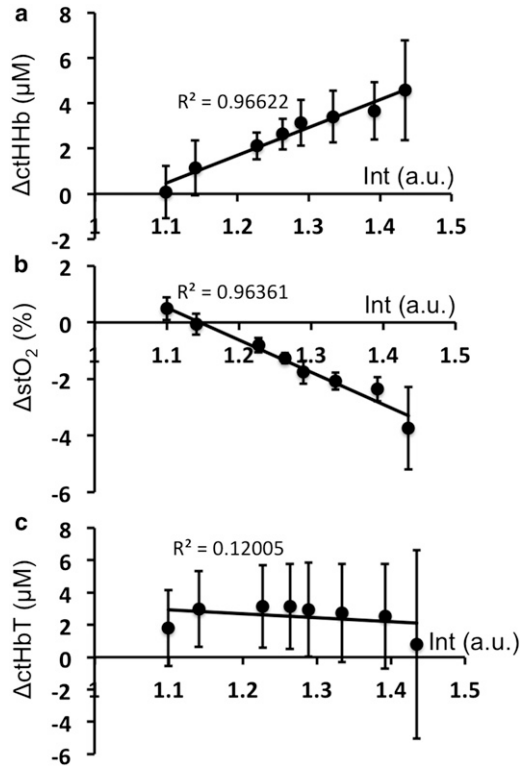

FIGURE 6 Relationship between the change in deoxyhemoglobin concentration ctHHb (*a*), hemoglobin oxygen saturation stO_2 (*b*), total oxyhemoglobin concentration ctHbT (*c*), and the change in the NADH fluorescence intensity (*Int*), during arterial occlusion. Error bars represent standard deviation.

Correlated changes in optical signals from NADH and hemoglobin during oxygen deprivation have been previously studied in cerebral cortex of a swine model (9) using a Mercury arc lamp as the excitation source. When measuring UV excitation-based NADH fluorescence, care needs to be taken to correct possible artifacts in the NADH fluorescence due to the light absorption by hemoglobin at both the excitation and fluorescence wavelengths. In two-photon-induced NADH fluorescence using NIR laser sources, this effect is negligible unless imaging in a blood-filled field. The reason for this is that the two-photon excitation is highly localized in the focal volume. Nevertheless, to fully address the concern regarding the impact of intrinsic tissue optical properties on in vivo nonlinear fluorescence, we considered two approaches: 1), We analyzed the absorption and scattering data obtained during the SFDI measurements throughout the occlusion to deduce whether there were significant measurable changes in the NADH emission spectral range: 450–550 nm; 2), We developed a Monte Carlo-based radiative transport model to simulate how the changes in absorption and scattering in blood-containing skin layers impact the NADH fluorescence collected by the objective during occlusion.

The absorption and scattering data obtained from a single SFDI measurement series at 658 nm are shown in Fig. 7. Error bars in Fig. 7 represent SFDI measurement standard deviation (39). During occlusion, we observed ~5–6% increase in absorption (due to deoxyhemoglobin sensitivity at this wavelength) and ~1% increase in scattering. We used the percentage changes in data obtained at all SFDI wavelengths to deduce whether there were significant changes in the NADH emission spectral range: 450–550 nm. For the scattering prediction, we applied well-established wavelength-dependent tissue scattering principles (40,41). To obtain the absorption coefficients, we used the recovered concentrations of Hb/HbO_2 from SFDI. Based on these chromophore values, the expected absorption in the spectral range: 450–550 nm was calculated using known absorption values of hemoglobin (42). Using these extrapolated results from SFDI measurements, no significant changes in

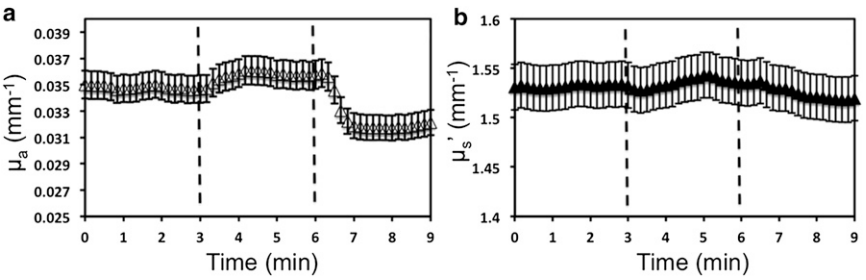

FIGURE 7 Absorption (*a*) and scattering (*b*) coefficients at 658 nm obtained from SFDI measurements. The dashed lines represent the start and the release points of the occlusion. Error bars represent SFDI measurement standard deviation (39).

absorption and scattering are seen at NADH emission wavelengths due to changes in oxy/deoxyhemoglobin during occlusion.

SFDI-measured optical properties are integrated over a much larger volume than MPM signals. As a result, this approach does not fully account for the possibility that highly localized optical property changes could influence the NADH fluorescence. To better understand this problem, we considered a 7-layer skin model (Fig. 3) with an embedded isotropic point source to simulate the NADH fluorescence emission. We simulated reflectance spectra using the skin properties and the skin model described previously in the Materials and Methods. We calculated the response of the reflectance spectra at three wavelengths (450, 500, and 550 nm) for the average change in scattering derived from SFDI (~1% increase) and in the hemodynamic coefficients (3.1 μM increase in Hb and 2.3 μM decrease in HbO_2) during occlusion measured with the SFDI. This change resulted in an increase of the absorption coefficients of the blood-filled skin layers in a range between 0.1% and 3.7%, depending on the layer and the wavelength, and less than a 1% increase in the reflectance spectra at all three wavelengths. The Monte Carlo simulation results show that changes in optical properties due to hemodynamic fluctuations during occlusion do not significantly affect detected NADH fluorescence measurements (<1%).

We ran simulations for significantly larger changes in absorption and scattering in the blood-containing skin layers to determine the degree to which the skin optical properties would have to change during the occlusion to account for an increase in NADH fluorescence comparable to what we measure during occlusion (~30%). Our simulations show that, for the position of our fluorescent source with respect to the blood filled layers, increases in scattering and/or decreases in absorption can increase the detected NADH fluorescence. However, the degree to which these optical properties would have to change to produce the observed 30% increase in fluorescence is extreme. For example, a 10-fold increase in scattering coefficient in the blood-containing skin layers during occlusion would result in an apparent increase in NADH fluorescence of only 18% at 450 nm, 26% at 500 nm, and 27% at 550 nm. Although this could have a significant impact on our measurements of the NADH fluorescence during occlusion, a 10-fold increase in scattering due to small variations in hemodynamics is not physiologically realistic and, to our knowledge, scattering fluctuations of this magnitude have not been reported in the literature regardless of technique (i.e., coherent or diffuse based spectroscopy/imaging). A 100-fold decrease in absorption would also result in an apparent increase in the NADH fluorescence by 12% at 450 nm, 9% at 500 nm, and 12% at 550 nm. The extreme reduction in absorption that would have to occur during ischemia is also unrealistic and inconsistent with known measurements.

Fig. 8 shows the results of Monte Carlo interrogation map simulations designed to gain an understanding of how the light interrogates various regions in the tissue before detection. The voxel dimensions were 5 μm along the *x* and *z* axes and infinite in extent along the *y* axis. The color of each

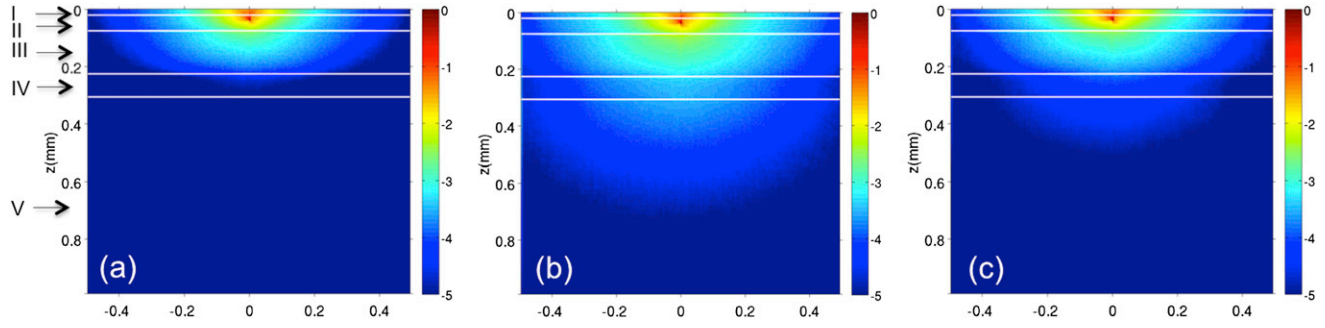

FIGURE 8 Interrogation maps showing the skin layers sampled by photons emitted by the fluorescent source corresponding to 450 nm (*a*), 500 nm (*b*), and 550 nm (*c*). The *z* axis represents the skin tissue depth (the origin is on the tissue surface). The white horizontal lines mark the separation between the skin layers considered in the Monte Carlo simulation. The colorbar is on a log scale with a spectrum ranging from 1 to 10^{-5}.

voxel represents the probability of visiting this voxel and ultimately being detected, P(V&D). The colorbar is on a log scale with a spectrum ranging from 1 to 10^{-5}. The white horizontal lines indicate the tissue layer interfaces. The width of each figure spans the diameter of the detector. Simulations are shown for 450, 500, and 550 nm light (Fig. 8, *a–c*, respectively). These figures illustrate that tissue regions sampled by photons emitted by the fluorescent source and subsequently detected are primarily confined to the upper two tissue layers (stratum corneum and epidermis). Photons that visit the blood-containing skin layers (papillary dermis and below) possess detected weights that are ~1000-fold smaller, on average. These plots help to explain why even extreme changes in the absorption and scattering properties of the blood-containing layers have little effect on the resulting measured signal. They also support why physiologically impossible changes to the optical properties in these layers are required to elicit an apparent 30% increase in NADH fluorescence during occlusion.

The correlation of changes in NADH fluorescence with changes in vascular hemoglobin during oxygen deprivation allows an estimation of the oxygen consumption rate by basal layer keratinocytes. From the average decrease in oxyhemoglobin concentration of 0.025 μmoles/L/s during the arterial occlusion measured by SFDI, the oxygen consumption rate can be estimated as 0.1 μmoles/L/s by using Eq. 1. By calculating the TPEF imaged volume of the keratinocytes close to the basal layer, the oxygen consumption rate of these cells can be estimated. Therefore, in the TPEF imaged volume of ~200 picoliters containing around 200 cells, the oxygen consumption rate can be estimated to be ~0.035 μmoles/10^6 cells/h. This is the first attempt, to our knowledge, to measure the oxygen consumption rate by human keratinocytes in vivo. Oxygen consumption rates in cell cultures have been measured previously for mammalian cells (0.05–0.5 μmoles/10^6 cells/h) (43), rat hepatocytes (1 μmole/10^6 cells/h) (44), rat bone marrow (0.02 μmoles/10^6 cells/h) (45), and human bone morrow (0.03 μmoles/10^6 cells/h) (46).

CONCLUSIONS

We have conducted noninvasive in vivo monitoring of changes in NADH fluorescence of epidermal keratinocytes during ischemia in a human subject. The results presented demonstrate, for the first time, to our knowledge, the depth dependent sensitivity of human epidermis to vascular oxygen supply. The changes in NADH fluorescence during arterial occlusion imply that the metabolic processes of keratinocytes close to the basal layer are regulated by vascular oxygen, whereas the keratinocytes in upper layers such as stratum granulosum are either supplied by atmospheric oxygen or are functionally anaerobic as suggested in previous studies. This outcome favors the concept of the vascular oxygen contribution to the basal layer of epidermis oxygen supply being significant (12) rather than negligible as suggested in a previous study (14).

The changes in NADH fluorescence of keratinocytes during occlusion were correlated to changes in tissue oxy- and deoxyhemoglobin concentration using SFDI. During occlusion, a decrease in oxyhemoglobin corresponded to an increase in NADH fluorescence of the basal epidermal cells. A multilayer Monte Carlo-based radiative transport model was developed to establish that localized tissue optical property changes during occlusion did not impact NADH fluorescence and could not explain the observed signal increase. Thus, the combined MPM/SFDI measurements allowed us to estimate an oxygen consumption rate of ~0.035 μmoles/10^6 cells/h in keratinocytes close to the basal layer. These studies provide a better understanding of the spatially varying metabolism of human epidermal cells and could be extended to in vivo measurements of oxygen metabolism in other tissues.

Support for this work was provided by the National Institutes of Health (NIH) NIBIB Laser Microbeam and Medical Program (LAMMP, P41-EB015890) and NIH K25-EB007309. Beckman Laser Institute programmatic support from the Arnold and Mabel Beckman Foundation and Air Force Research Laboratory Agreement No. FA9550-04-1-0101 is acknowledged.

Karsten König is cofounder of JenLab GmbH, Amaan Mazhar is an employee of Modulated Imaging, and Bruce Tromberg is a cofounder of Modulated Imaging.

REFERENCES

1. Chance, B., and H. Baltscheffsky. 1958. Respiratory enzymes in oxidative phosphorylation. VII. Binding of intramitochondrial reduced pyridine nucleotide. *J. Biol. Chem.* 233:736–739.
2. Chance, B., N. Oshino, …, A. Mayevsky. 1973. Basic principles of tissue oxygen determination from mitochondrial signals. *Adv. Exp. Med. Biol.* 37A:277–292.
3. Mayevsky, A., and G. G. Rogatsky. 2007. Mitochondrial function in vivo evaluated by NADH fluorescence: from animal models to human studies. *Am. J. Physiol. Cell Physiol.* 292:C615–C640.
4. Obi-Tabot, E. T., L. M. Hanrahan, …, W. W. LaMorte. 1993. Changes in hepatocyte NADH fluorescence during prolonged hypoxia. *J. Surg. Res.* 55:575–580.
5. Foster, K. A., C. J. Beaver, and D. A. Turner. 2005. Interaction between tissue oxygen tension and NADH imaging during synaptic stimulation and hypoxia in rat hippocampal slices. *Neuroscience.* 132:645–657.
6. Scholz, R., R. G. Thurman, …, T. Bücher. 1969. Flavin and pyridine nucleotide oxidation-reduction changes in perfused rat liver. I. Anoxia and subcellular localization of fluorescent flavoproteins. *J. Biol. Chem.* 244:2317–2324.
7. Ji, S. C., J. J. Lemasters, V. Christenson, and R. G. Thurman. 1982. Periportal and pericentral pyridine-nucleotide fluorescence from the surface of the perfused liver: evaluation of the hypothesis that chronic treatment with ethanol produces pericentral hypoxia. *Proc. Natl. Acad. Sci. USA.* 79:5415–5419.
8. Mayevsky, A., S. Lebourdais, and B. Chance. 1980. The interrelation between brain PO2 and NADH oxidation-reduction state in the gerbil. *J. Neurosci. Res.* 5:173–182.
9. Rampil, I. J., L. Litt, and A. Mayevsky. 1992. Correlated, simultaneous, multiple-wavelength optical monitoring in vivo of localized

cerebrocortical NADH and brain microvessel hemoglobin oxygen saturation. *J. Clin. Monit.* 8:216–225.

10. Pappajohn, D. J., R. Penneys, and B. Chance. 1972. NADH spectrofluorometry of rat skin. *J. Appl. Physiol.* 33:684–687.
11. Cordeiro, P. G., R. E. Kirschner, …, D. A. Hidalgo. 1995. Ultraviolet excitation fluorescence spectroscopy: a noninvasive method for the measurement of redox changes in ischemic myocutaneous flaps. *Plast. Reconstr. Surg.* 96:673–680.
12. Palero, J. A., A. N. Bader, …, H. C. Gerritsen. 2011. In vivo monitoring of protein-bound and free NADH during ischemia by nonlinear spectral imaging microscopy. *Biomed. Opt. Express.* 2:1030–1039.
13. Sanchez, W. Y., T. W. Prow, …, M. S. Roberts. 2010. Analysis of the metabolic deterioration of ex vivo skin from ischemic necrosis through the imaging of intracellular NAD(P)H by multiphoton tomography and fluorescence lifetime imaging microscopy. *J. Biomed. Opt.* 15:046008.
14. Stücker, M., A. Struk, …, D. W. Lübbers. 2002. The cutaneous uptake of atmospheric oxygen contributes significantly to the oxygen supply of human dermis and epidermis. *J. Physiol.* 538:985–994.
15. Ronquist, G., A. Andersson, …, B. Falck. 2003. Human epidermal energy metabolism is functionally anaerobic. *Exp. Dermatol.* 12: 572–579.
16. Konig, K., and I. Riemann. 2003. High-resolution multiphoton tomography of human skin with subcellular spatial resolution and picosecond time resolution. *J. Biomed. Opt.* 8:432–439.
17. Mazhar, A., S. Dell, …, B. J. Tromberg. 2010. Wavelength optimization for rapid chromophore mapping using spatial frequency domain imaging. *J. Biomed. Opt.* 15:061716.
18. Huang, S., A. A. Heikal, and W. W. Webb. 2002. Two-photon fluorescence spectroscopy and microscopy of NAD(P)H and flavoprotein. *Biophys. J.* 82:2811–2825.
19. Heikal, A. A. 2010. Intracellular coenzymes as natural biomarkers for metabolic activities and mitochondrial anomalies. *Biomarkers Med.* 4:241–263.
20. Weber, G. 1950. Fluorescence of riboflavin and flavin-adenine dinucleotide. *Biochem. J.* 47:114–121.
21. Rocheleau, J. V., W. S. Head, and D. W. Piston. 2004. Quantitative NAD(P)H/flavoprotein autofluorescence imaging reveals metabolic mechanisms of pancreatic islet pyruvate response. *J. Biol. Chem.* 279:31780–31787.
22. Patterson, G. H., S. M. Knobel, …, D. W. Piston. 2000. Separation of the glucose-stimulated cytoplasmic and mitochondrial NAD(P)H responses in pancreatic islet beta cells. *Proc. Natl. Acad. Sci. USA.* 97:5203–5207.
23. Cuccia, D. J. 2012. Spatial frequency domain imaging (SFDI): a technology overview and validation of an LED-based clinic friendly device. *Proc. SPIE.* 8254:825405–825406.
24. Gioux, S., A. Mazhar, …, J. V. Frangioni. 2009. Three-dimensional surface profile intensity correction for spatially modulated imaging. *J. Biomed. Opt.* 14:034045.
25. Konecky, S. D., A. Mazhar, …, B. J. Tromberg. 2009. Quantitative optical tomography of sub-surface heterogeneities using spatially modulated structured light. *Opt. Express.* 17:14780–14790.
26. Boas, D. A., and M. A. Franceschini. 2011. Haemoglobin oxygen saturation as a biomarker: the problem and a solution. *Philos. Transact. A Math. Phys. Eng. Sci.* 369:4407–4424.
27. Meglinski, I. V., and S. J. Matcher. 2002. Quantitative assessment of skin layers absorption and skin reflectance spectra simulation in the visible and near-infrared spectral regions. *Physiol. Meas.* 23:741–753.
28. van Gemert, M. J., S. L. Jacques, …, W. M. Star. 1989. Skin optics. *IEEE Trans. Biomed. Eng.* 36:1146–1154.
29. Virtual Photonics Technology Initiative. http://www.virtualphotonics.codeplex.com. Accessed August 10, 2012.
30. Wang, L. H., S. L. Jacques, and L. Q. Zheng. 1995. Mcml - Monte-Carlo modeling of light transport in multilayered tissues. *Comput. Meth. Prog. Bio.* 47:131–146.
31. Hayakawa, C. K., J. Spanier, and V. Venugopalan. 2007. Coupled forward-adjoint Monte Carlo simulations of radiative transport for the study of optical probe design in heterogeneous tissues. *SIAM J. Appl. Math.* 68:253–270.
32. Lehninger, A. L., D. L. Nelson, and M. M. Cox. 2008. Lehninger Principles of Biochemistry. W. H. Freeman, New York.
33. Lübbers, D. W. 1994. Microcirculation and O2 exchange through the skin surface: a theoretical analysis. *Adv. Exp. Med. Biol.* 361:51–58.
34. Grossmann, U. 1982. Simulation of combined transfer of oxygen and heat through the skin using a capillary-loop model. *Math. Biosci.* 61:205–236.
35. Stücker, M., P. A. Struk, …, D. W. Lübbers. 2000. The transepidermal oxygen flux from the environment is in balance with the capillary oxygen supply. *J. Invest. Dermatol.* 114:533–540.
36. Ivarsson, R., R. Quintens, …, F. C. Schuit. 2005. Redox control of exocytosis: regulatory role of NADPH, thioredoxin, and glutaredoxin. *Diabetes.* 54:2132–2142.
37. Garofalo, O., D. W. Cox, and H. S. Bachelard. 1988. Brain levels of NADH and NAD+ under hypoxic and hypoglycaemic conditions in vitro. *J. Neurochem.* 51:172–176.
38. Nishidate, I., N. Tanaka, …, K. Niizeki. 2011. Noninvasive imaging of human skin hemodynamics using a digital red-green-blue camera. *J. Biomed. Opt.* 16:086012.
39. Cuccia, D. J., F. Bevilacqua, …, B. J. Tromberg. 2009. Quantitation and mapping of tissue optical properties using modulated imaging. *J. Biomed. Opt.* 14:024012.
40. Saidi, I. S., S. L. Jacques, and F. K. Tittel. 1995. Mie and Rayleigh modeling of visible-light scattering in neonatal skin. *Appl. Opt.* 34:7410–7418.
41. Mourant, J. R., T. Fuselier, …, I. J. Bigio. 1997. Predictions and measurements of scattering and absorption over broad wavelength ranges in tissue phantoms. *Appl. Opt.* 36:949–957.
42. Prahl, S., Optical absorption of hemoglobin. http://omlc.ogi.edu/spectra/hemoglobin/ Accessed August 10, 2012.
43. Miller, W. M., and H. W. Blanch. 1991. Regulation of animal cell metabolism in bioreactors. *Biotechnology.* 17:119–161.
44. Rotem, A., M. Toner, …, M. L. Yarmush. 1992. Oxygen uptake rates in cultured rat hepatocytes. *Biotechnol. Bioeng.* 40:1286–1291.
45. Gesinski, R. M., J. H. Morrison, and J. R. Toepfer. 1968. Measurement of oxygen consumption of rat bone marrow cells by a polarographic method. *J. Appl. Physiol.* 24:751–754.
46. Peng, C. A., and B. O. Palsson. 1996. Determination of specific oxygen uptake rates in human hematopoietic cultures and implications for bioreactor design. *Ann. Biomed. Eng.* 24:373–381.